Dynamics of foams with and without wall rupture

J. J. Chae
Department of Physics, University of Arizona, Tucson, Arizona 85721

M. Tabor
Program in Applied Mathematics, University of Arizona, Tucson, Arizona 85721

(Received 12 February 1996; revised manuscript received 2 August 1996)

A physically based model for the evolution of dry, two-dimensional foams based on a combination of mass transfer, vertex movement, and edge relaxation, enables efficient and accurate simulation with and without wall rupture. The stochastic nature of topological transitions due to numerical error has been carefully examined and may explain the discrepancies found among various simulations. The separation of vertex and edge movements permits a study of foam evolution that includes wall rupture. Comparison with recent experimental results is presented that demonstrates that certain, semiempirical ''breaking rules'' are capable of reproducing both the overall topological evolution and certain scaling behavior observed in the experiments. [S1063-651X(96)09012-5]

PACS number(s): 82.70.Rr, 83.70.Hq

I. INTRODUCTION

The structure and evolution of cellular assemblies, especially foams of soap bubbles, has long been a source of fascination and scientific study. In particular, two-dimensional foams have been recognized as valuable analogs of grain boundaries in metals; and have the obvious advantage of being relatively easy to study experimentally and, more recently, simulate numerically. The past ten years has seen an intensification of effort to obtain a (reasonably) complete experimental, theoretical and numerical picture of two-dimensional soap foam evolution. One of the central issues has been to establish the existence of a ''scaling regime'' in which the probability distributions characterizing the statistical structure of the foam are stationary and to measure, either experimentally and/or through simulation, the appropriate exponent and moments in this regime.

The basic phenomenology of two-dimensional foam evolution is well established—at least in the case of foams that are relatively ''dry'' (i.e., contain virtually no fluid) and in which wall rupture does not occur. We shall refer to such foams as ''normal'' foams to distinguish them from what we will term ''breaking'' foams in which wall rupture is a major part of the evolution. The study of this class of foam dynamics, which is very different (and much faster) from that of normal foams, is one of our main objectives. Before discussing this further we summarize some of the basic ideas involved in normal foam evolution. The principal driving force is diffusion, namely, gas molecules diffusing across the curved cell walls between bubbles. The pressure difference across these walls is governed by the Young-Laplace law

$$\Delta P = \frac{2\sigma}{r}, \tag{1}$$

where σ is the coefficient of surface tension and r the radius of curvature of the wall. Based on this law and elementary geometric considerations, which include the assumption that in equilibrium the cell walls meet at 120°, von Neumann [1] deduced a simple law governing cell growth, namely,

$$\frac{da_n}{dt} = \kappa(n-6), \tag{2}$$

where a_n is the area of an n-sided cell and κ is a diffusion constant. Thus cells with more than six sides grow in area and those with less than six sides shrink. By itself this law cannot fully explain typical foam evolution since additional topological processes corresponding to various types of wall rearrangements also occur. For example, as four- and five-sided bubbles shrink according to von Neumann's law, a point of zero area will be reached creating vertices with, respectively, four and five cell walls meeting at a point. Since the stable coordination number (the number of edges meeting at a vertex) is three, there must be wall rearrangements to reestablish this configuration. These rearrangements are called $T2$ processes and are illustrated in Fig. 1. In addition, as also shown, one can identify a somewhat different transition involving wall switching which is called a $T1$ process. Both of these processes play an important part in the foam evolution and, as we will discuss below, behavior in the scaling regime is sensitive to small variations in the occurrence of these transitions. This is the notion of ''stochasticity'' in foam evolution raised by Fradkov *et al.* [2]. It should also be noted that one of the assumptions in von Neumann's law is that the pressure differences across the walls are small compared to the pressure in the domains [3].

During the course of evolution, various statistical measures of the cellular structure can be followed (either in an actual laboratory experiment or in a computer simulation). These include $\rho(n,t)$, the probability of finding an n-sided cell, and $\rho(a,t)da$, the probability of finding a cell area between a and $a+da$. A useful statistic is provided by the second moment, $\mu_2 = \Sigma(n-6)^2\rho(n,t)$, which gives a simple measure of the system disorder (a monodisperse hexagonal foam, for which μ_2 is obviously zero, is considered to be a highly ordered structure). Over the years various experiments

 © 1997 The American Physical Society

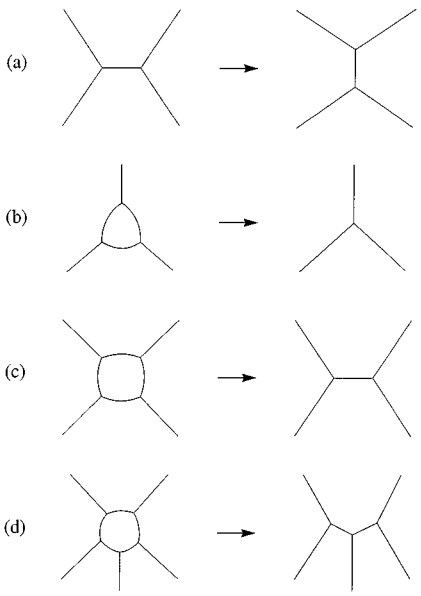

FIG. 1. Topological transitions in two-dimensional foams. (a) $T1$ transition—wall switching. (b)–(d) $T2$ transition of three-, four-, and five-sided cell, respectively.

(much of the published literature on two-dimensional foam kinetics is well summarized in the reviews by Glazier and Weaire [4] and Stavans [5]) have established that there is indeed a scaling regime in which $\langle a \rangle$ grows linearly with t and that the various statistical quantities are stationary. We comment, however, that it appears to be easier to establish stationarity for $\rho(n,t)$ than for $\rho(a,t)$. One problem in obtaining accurate experimental results is that of foam wetness, i.e., the accumulation of liquid in the vertices. This leads to the formation of ''Plateau borders'' with subsequent effects on the idealized von Neumann law dynamics [6]. Another hallmark of a scaling regime is the constancy of μ_2: experimental observations indicate a value of approximately 1.4. In our computer simulations of normal foams we will show, in particular, the sensitivity of μ_2 to the topological transitions.

Numerical simulation of evolving foams is a challenging problem in large-scale scientific computation. Surveys of the various approaches can be found in [4,5,7]. Although certain ''nonphysical'' models such as the Potts model are computationally inexpensive and can reproduce some of the basic evolution phenomenology, it is important to develop algorithms that can simulate the actual physics of foam evolution. This is a difficult problem since one must, in principle, follow the movement of all cell walls and vertices simultaneously. To date, the main two efforts in this direction are due to Weaire and Kermode [8,9] (henceforth referred to as WK) and Aref and Herdtle [10,11] (henceforth referred to as AH). Both approaches trace the quasiequilibrium configurations, i.e., configurations in which all edges meet at 120° and the net pressure across each edge is zero. The adjustments needed to attain these arrangements are implemented after each ''diffusion step'' in which the area changes according to von Neumann's law. In both algorithms the vertex and edge adjustments are effected via a Jacobian matrix approach. The most important difference between WK and AH is that the latter computes the relaxation with the (very large) Jacobian corresponding to the entire network of bubbles whereas WK breaks the Jacobian into small (5×5) blocks (corresponding to one vertex and its local environment of three surrounding cells) and carrying out the relaxation one sub-block at a time. This becomes significant at the level of the $T1$ transitions: WK apply their criteria for allowing such transitions at the local (sub-block) level whereas AH apply their criteria at the global level, i.e., after the entire network has completed a relaxation step. As pointed out in [11] the local approach can lead to spurious $T1$ transitions with corresponding implications for long-range correlations in the foam dynamics. On the other hand, the disadvantage of the AH approach is the inevitable increase in computational time that goes with manipulating very large matrices.

Here our aim is to simulate foam evolution in a way that permits description of a wide range of behaviors: such as accurate normal foam evolution; breaking foams in which wall rupture is a frequent event; the inclusion of anisotropy (i.e., variations in surface energy according to cell orientation) to enable modeling of grain boundaries; and at the same time have sufficient control over the detailed dynamics to permit accurate investigation of stochastic effects in the topological transition, etc. To be able to achieve this the simulation must work with a physically realistic model of evolution in which pressure, gas mass, edge, and vertex motions are all explicitly and independently taken into account in a way that is also efficient enough to allow routine studies of systems with large numbers of cells.

Below we describe our model of foam evolution and its algorithmic implementation. The model combines physically realistic vertex motion with edge readjustments governed by the Young-Laplace law and mass diffusion governed by a von Neumann–like law in a way that is appropriate for the study of both normal and breaking foams. Selected new results for normal foams, such as a study of stochastic effects, illustrate the effectiveness of the algorithm. These results are followed by the simulation studies of breaking foams.

II. MODEL AND ALGORITHMS

The relaxation from a nonequilibrium to a quasiequilibrium state in a two-dimensional foam is completely determined by the dynamics of the vertices and edges of the bubbles. In a normal foam, the relaxation takes place after the gas diffuses from (in general) small bubbles to large bubbles; and in a breaking foam, after the wall ruptures. A physically realistic model ([12,13]) for vertex motion is to represent the driving force on a vertex as the sum of the elastic forces generated by the three films that meet at that vertex. If we assume that (i) the surface tension of the film is constant throughout the foam, (ii) the motion of films is purely dissipative [12], and (iii) the mobility (by ''mobility'' we mean the inverse of the friction coefficient) per unit length of the soap film is isotropic and constant; the velocity of the ith vertex is given by [13]

$$\mathbf{v}_{i,v} = \frac{2\sigma\mu h \sum_{(j)\ \text{neighbors}} \mathbf{u}_{ij}}{\sum_{(j)\ \text{neighbors}} l_{ij}}, \tag{3}$$

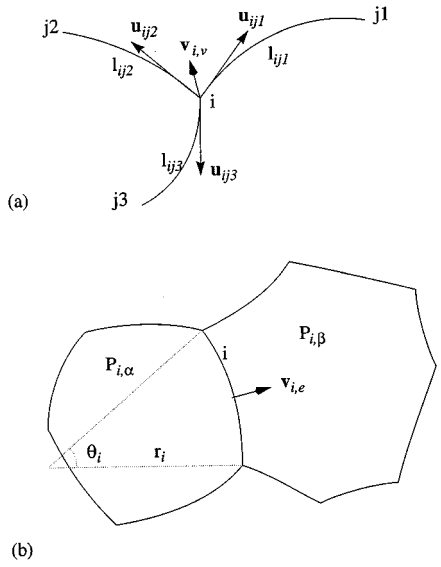

FIG. 2. Local geometry and parameters of (a) a vertex, and (b) an edge.

where σ and μ denote, respectively, the surface tension and mobility per unit length of the soap film, and h is the narrow gap between two plates of the experimental cell. The $\mathbf{u}_{ij}$ is the unit vector attached to the ith vertex and tangent to the film joining the ith and jth vertices, and the length of this film is l_{ij} [see Fig. 2(a)]. The effect of velocities of neighboring vertices on $\mathbf{v}_{i,v}$ [13] is not considered in Eq. (3).

In the vertex models of foam evolution (in which the foam is treated as simply a network of connected vertices) studied by Nakashima, Nagai, and Kawasaki [13], three different vertex velocities were investigated. In these the vertex velocity is (i) inversely proportional to the mean edge length in the entire foam; (ii) inversely proportional to the sum of the three edge lengths meeting at the vertex in question; or (iii) inversely proportional to the sum of the three edge lengths projected onto a line normal to the force vector acting at that vertex [14]. These different choices of velocity induce different network evolutions since, in the vertex model, the coarsening (i.e., growth and disappearance of bubbles) of a foam is driven exclusively by the vertex movements. By contrast, in our model vertex movement is just one part of the two-step relaxation process (the other step being edge adjustment) during which a nonequilibrium configuration returns to a quasiequilibrium one while the actual coarsening is handled in a separate diffusion step. Comparison tests in our model of all three different choices of vertex velocity gave overall foam evolution results that were identical to within a negligible range of errors.

The motion of an edge is, in principle, determined by the net force per unit area, given the mobility and the height of a soap film. The magnitude of this force, which we will refer to as the ''net pressure,'' on the ith edge, P_i^{net}, is given by

$$P_i^{\text{net}} = P_{i,\alpha} - P_{i,\beta} - 2\frac{\sigma}{r_i}, \tag{4}$$

where $P_{i,\alpha} - P_{i,\beta}$ is the pressure difference across the ith edge (the left-hand and right-hand domains of the ith edge are labeled as the α and β domains, respectively), and r_i is the radius of curvature of that edge as shown in Fig. 2(b). Given P_i^{net}, the velocity of the center of the ith edge $\mathbf{v}_{i,e}$ is given by

$$\mathbf{v}_{i,e} = \hat{\mathbf{n}}_i \mu h P_i^{\text{net}}, \tag{5}$$

where $\hat{\mathbf{n}}_i$ is unit normal vector at the center of the edge. However, as we now argue, this last equation does not need to be used to obtain physically realistic edge adjustments.

In typical experimental conditions, where the pressure of the gas and the surface tension of the film are of order 10^6 g/sec^2 cm and 10^2 g/sec^2, respectively, Eqs. (3) and (5) show that the elastic relaxation of the edges is rapid compared to that of the vertices. This is also observed in the breaking-foam experiments [15]. Therefore, it is reasonable to assume that the edges are in equilibrium between each movement of the vertices. As a consequence, the edge velocity in Eq. (5) is not employed explicitly in our algorithm and instead the radius of curvature of each edge is enforced to be in equilibrium between each movement of the vertices, i.e., we adjust the radius to satisfy Eq. (4). We can think of this as a ''geometrical,'' rather than ''dynamical'' approach to the edge adjustment part of the relaxation process. We also note, as shown in Fig. 2(b), that the variable that we use to specify the curvature of the ith edge is chosen to be an ''opening angle'' θ_i of the ith circular edge rather than the radius because edges whose opening angles are bigger than 180° are commonly observed in a breaking-foam experiment [15].

A. Simulation of normal foams

Coarsening of a normal foam is due to the gas diffusion from higher-pressure domains to lower-pressure domains, followed by the elastic relaxation of the edges and vertices, which can be assumed to occur almost instantaneously because the gas diffusion is much slower than the elastic relaxation. Although von Neumann's law is usually formulated in terms of area and assumes incompressibility of the gas, we assume the ideal gas law and formulate it in terms of gas ''mass,'' i.e., the number of gas molecules, in the bubble. The diffusion rate of gas through the ith edge $R_{i,d}$ is proportional to the pressure difference ΔP_i across the ith edge and length of the ith edge, i.e.,

$$R_{i,d} \propto l_i \Delta P_i . \tag{6}$$

Equation (6) and the considerations described in Sec. I give the analogue of von Neumann's law for ''mass transfer,'' namely,

$$\frac{dM_n}{dt} = k(n-6), \tag{7}$$

where n and M_n are the number of sides and mass of the bubble, respectively, and k is a coefficient proportional to the diffusion constant κ in Eq. (2).

The overall evolution of a normal foam proceeds in the following way. During a ''diffusion step'' of duration Δt_D, bubbles lose or gain mass according to Eq. (7). After the diffusion step, a readjustment of the curvature of each edge is required because the mass and pressure in each bubble will

have changed to new values and, furthermore, this curvature adjustment will result in the angles between neighboring edges deviating from 120°. Accordingly, following the diffusion step, a two-part ''relaxation step'' is implemented which consists of (i) moving all vertices, according to Eq. (3), at the same time in a time step Δt_r and (ii) readjusting the curvature of each edge while all vertices are fixed. These two steps are performed alternately until the quasiequilibrium configuration of the foam is reached and then the next diffusion step is implemented.

The possible occurrence of a $T2$ transition during the diffusion step and a $T1$ transition during the relaxation step, plus several other considerations, are involved in determining optimal values of the Δt_D and Δt_r. In the latter case, all the vertex motions have to be monitored with care since a collision between vertices heralds the onset of a $T1$ transition and unphysical phenomena such as repeated oscillations of these transitions, which can occur in numerical simulations [13], have to be avoided. Overall, we are able to implement a series of criteria for estimating the time steps in a way which eliminates spurious behavior and/or loss of convergence and enables rather tight control on the accuracy and form of the topological transitions. A detailed discussion of these considerations and many other algorithmic details is given in [7].

As stated above the relaxation step consists of alternate vertex movements and curvature adjustments. The latter are implemented by eliminating the net pressures, as governed by Eq. (4), on all edges. Since the positions of the vertices and the masses of the domains are assumed to remain fixed while the edges move, the pressure of a domain is a function of its opening angles. The change in the net pressure on the ith edge, dP_i^{net}, can be derived from Eq. (4) in terms of the change in the opening angle of that edge, $d\theta_i$:

$$dP_i^{\text{net}} = \sum_j \frac{\partial P_{i,\alpha}}{\partial \theta_j} d\theta_j - \sum_{j'} \frac{\partial P_{i,\beta}}{\partial \theta_{j'}} d\theta_{j'} + \frac{2\sigma}{r_i^2} \frac{\partial r_i}{\partial \theta_i} d\theta_i , \tag{8}$$

where the sum is over the edges of the α and β domains, respectively [see Fig. 2(b)]. Given the net pressures on the edges, $d\theta_i$ can be calculated from Eq. (8), which in turn is subtracted from the current θ_i to obtain the new θ_i.

For large systems solution of Eq. (8) can become computationally expensive. In contrast to the direct, Jacobian-matrix approaches used in the AH and WK algorithms, we use an iterative method in the form of a multidimensional Newton-Raphson method with a diagonal preconditioner. The basic procedure consists of changing the curvature (i.e., the opening angle θ) of each edge in sequence, and repeating this until the desired accuracy is achieved. Thus, if the curvatures of all edges except the ith edge are stationary, the change in θ_i to eliminate the net pressure on the ith edge can be derived from Eq. (8), namely,

$$d\theta_i = dP_i^{\text{net}} \Big/ \left(\frac{\partial P_{i,\alpha}}{\partial \theta_i} - \frac{\partial P_{i,\beta}}{\partial \theta_i} + \frac{2\sigma}{r_i^2} \frac{\partial r_i}{\partial \theta_i} \right). \tag{9}$$

As WK pointed out, the complete elimination of the net pressure on each edge can drive the configuration of a foam far from equilibrium. Based on extensive numerical trials [7], the best convergence is achieved when we change θ_i by an amount corresponding to $d\theta_i$ divided by the average number of sides of the two domains that share the ith edge.

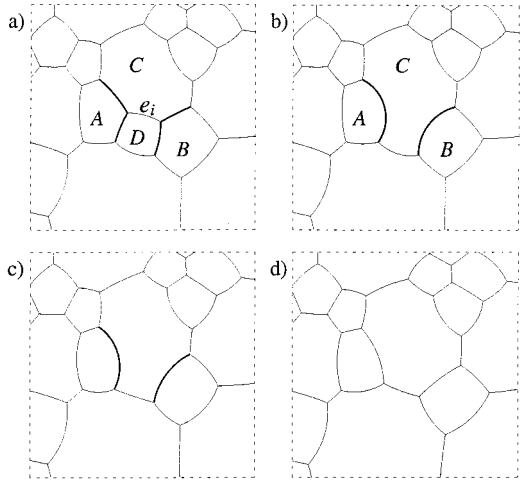

FIG. 3. Sequential stages of relaxation after the breakage of edge e_i; (a) prior to breakage, (b) immediately after breakage, (c) after the readjustments of curvature, and (d) after the foam reestablishes quasiequilibrium.

B. Simulation of breaking foam

One of our main objectives is to develop an algorithm suitable for the simulation of breaking foams. These have only recently been studied experimentally by Burnett *et al.* [15] and exhibit many differences from normal foams. The fundamental difference is that of time scale: a normal foam evolves over periods of tens of hours whereas a rupturing foam disintegrates in minutes. Typically, after a finite period of relatively few wall ruptures a ''cascade regime'' sets in, in which many frequent and even simultaneous breakings occur. Thus diffusion, the rate-determining process in normal foams, is no longer relevant and the evolution is dominated by the rapid transmission of stresses through the disintegrating network. As a consequence, many of the phenomena associated with normal foam evolution, such as universal scaling behavior, are no longer seen. However, as we will describe in Sec. IV, a new type of scaling regime may appear.

As discussed above in the algorithm for a normal foam we assume that a foam recovers a quasiequilibrium configuration between diffusion steps. By contrast, in the case of a breaking foam, we cannot assume this prior to a wall rupture because the time interval between successive breakings may not be long enough for a nonequilibrium configuration to relax back to a quasiequilibrium one. However, our approach of tracking the motion of all vertices and edges at any instant means that the breakdown cascade is easily followed by considering each wall rupture as a process of eliminating a selected edge. Consider the ith edge, e_i in Fig. 3(a). After the breaking of e_i, two pairs of edges that were connected to e_i become two new edges as illustrated with thick lines in Figs. 3(a) and 3(b). The curvature of each newly created edge is adjusted such that the areas of the A and B domains in Fig.

3(b) remain constant. The C and D domains combine to form a new, enlarged C domain with new values of area, mass, and pressure. The relaxation process is applied just as in normal foams; namely, the readjustments of curvature [Fig. 3(c)], and the movement of vertices are effected alternately until the next breaking occurs. Figure 3(d) shows the equilibrium configuration after complete elastic relaxation from Fig. 3(c). This capability of handling a nonequilibrium configuration is an advantage over the algorithms of WK and AH in which only the quasiequilibrium configurations are traced.

The actual physics of the wall rupture in the experiments is not well understood and in our simulations, we choose certain (semiphenomenological) ''static'' breaking rules, i.e., rules that depend in some way on the length of an edge rather than its velocity. The consequence of this is that even as a region of the foam is relaxing rapidly around a given rupture, the choice of the next rupture can be made without being unduly influenced by its predecessor. Therefore, successive ruptures can occur relatively remotely from each other—a behavior that is consistent with the experimental observations. Although there are undoubtedly some long-range correlations between successive ruptures, we adopt the following three simple breaking rules in which the probability of a given edge breaking is (i) random, (ii) proportional to the length of its edge, and (iii) proportional to the square of the length of its edge. The motivation for rule (ii) is provided by the observation that the average bursting time for a static soap bubble is inversely proportional to its surface area [16]; and the other rules are introduced for comparison.

Another difficulty in a breaking-foam simulation lies in determining the time interval between successive breaks—again due to the current lack of understanding of the precise mechanisms governing the wall rupture. In our current simulations, the time interval between breakings Δt_B is chosen randomly between 0 and $2\times\Delta t_{B,\mathrm{avg}}$, where $\Delta t_{B,\mathrm{avg}}$ denotes a user-specified average period between breakings. Although this ''rule'' for the time interval agrees with the experimental observation [15] in the ''cascade regime''—in which the number of bubbles decreases linearly in time—it cannot provide true, real time, breaking-foam dynamics. However, the numerical results can still be compared with those of experiment in terms of ''topological evolution''; namely, following the evolution as a function of bubble number rather than of real time.

III. NUMERICAL RESULTS FOR NORMAL FOAM EVOLUTION

We now present a number of simulation results for normal foams that illustrate the effectiveness of our algorithm and/or reveal differences with results obtained in other numerical studies. Frequently we will use two basic statistical measures of the structure of a foam: the side distribution $\rho(n)$ and the normalized area distribution $\rho(a/\langle a\rangle)$. The mth moments of these distributions are, respectively,

$$\mu_m=\sum_n \rho(n)(n-\langle n\rangle)^m, \tag{10}$$

$$\mu_m^A=\int \rho(a/\langle a\rangle)(a/\langle a\rangle-1)^m d(a/\langle a\rangle), \tag{11}$$

where $\langle n\rangle$ is the average number of sides of a bubble and $\langle a\rangle$ is the mean bubble area.

A. Initial conditions, pressure effects, and efficiency

The Voronoi construction has long been recognized as a very useful way of generating initial conditions for foam simulations (as well as other problems involving tilings of the plane). The standard construction (see, for example, [17] or [13]) involves building the cells about points deposited randomly in the plane. It is possible to produce different networks by imposing a ''hard-core'' constraint on these points, namely, setting a minimum distance on their separation. The larger the core, the less disordered the structure. For the simulation of foams presented here, we use doubly periodic Voronoi networks with large, small, or no hard cores. However, normally constructed Voronoi networks cannot be used directly as initial foam structures since Voronoi cell walls usually do not meet at 120°. To obtain the actual initial bubble structures from these Voronoi networks, a uniform initial pressure P_0 is assigned on each cell and then the relaxation process described in Sec. II is implemented. The resulting structure, however, varies with the assigned initial pressure whereas in the case of incompressible gas, only one relaxed structure exists for a given Voronoi network.

In the actual simulations, Eq. (4) is reformulated in terms of dimensionless parameters, namely,

$$\widetilde{P}_i^{\mathrm{net}}=\widetilde{P}_{i,\alpha}-\widetilde{P}_{i,\beta}-\frac{2}{\widetilde{r}_i}, \tag{12a}$$

$$\widetilde{P}=\frac{P}{(\sigma/h)}, \tag{12b}$$

$$\widetilde{r}_i=r_i/h. \tag{12c}$$

Thus, for actual laboratory experiments run at normal pressure with typical soap concentrations and cell separations, the initial dimensionless pressure $\widetilde{P}_0$ is usually of order 10^4. This large value of $\widetilde{P}_0$ significantly slows down the speed of the simulation. However, we have found that von Neumann's law (2) is well satisfied (typically to within 1%) at much lower values of $\widetilde{P}_0$ (say, no smaller than $\widetilde{P}_0=10^2$, i.e., $P_0\simeq 10^{-2}$ atm) and providing this is the case, runs at this low pressure ($P_0\simeq 10^{-2}$ atm) are essentially equivalent to those at normal pressure. The only noticable trend is that foams with lower pressure tend to have larger values of μ_2 than those with higher pressure [7]. We mention in passing that some unusual effects can be observed in simulations involving very low initial pressures. For example, at $P_0\simeq 10^{-5}$ atm, Voronoi networks of 1024 bubbles with either large, small, or no hard cores, were found never to relax to equilibrium configurations. In addition, by the time the initial pressure is reduced to $P_0\simeq 10^{-4}$ atm, significant deviations from von Neumann's law are observable [7]. We

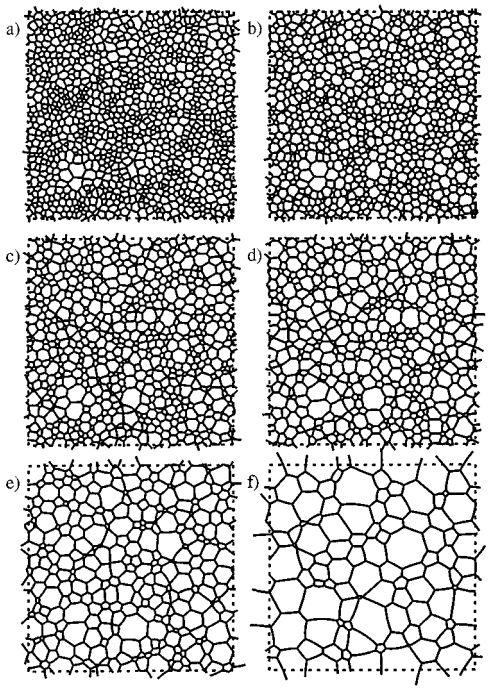

FIG. 4. A typical sequence of structures in the coarsening of a normal foam (run viii). Number of bubbles in (a)–(f) are 1024, 899, 704, 503, 297, and 100.

comment that another way of regarding foam evolution at different (initial) pressures is that, as seen in Eq. (12b), increasing the surface tension of a soap film is equivalent to decreasing the pressure.

In Fig. 4, we show a typical evolution sequence that starts with a relaxed small-core Voronoi network with $P_0 = 10^{-2}$ atm. Such a sequence is typical of the topological changes seen in an evolving normal foam.

This is an appropriate point to discuss the efficiency of our algorithm. The typical CPU time used for one bubble disappearance in a run such as above (Fig. 4), is found to scale as $O(N^{0.5-0.6})$ (where N is the current bubble number), in contrast to $O(N^{1.3})$ exhibited by AH's algorithm (WK did not report this data). All our simulations were performed on workstation computers and the typical CPU time used for 1024 bubbles to relax to 100 bubbles is approximately 150 h on a SPARCstation 20 with a single processor. A similar calculation by the AH algorithm requires approximately 30 h of Cray-YMP time.

Finally, in Table I, we summarize all the runs and initial configurations used in our foam simulations. Without changing the geometry, a different initial configuration (e.g., runs ii and iii) can be generated by changing the (equal) pressure added to each cell. In the various results described below, the ''run'' number identifies the details of the initial conditions used and can be read off this table.

B. Numerical stability and effects of stochasticity

The idea of ''stochasticity'' in two-dimensional soap foam has been recently discussed by Fradkov *et al.* [2]. Their paper describes how a foam can evolve to more than one configuration when a four- or five-sided cell vanishes. As shown in Fig. 5, for instance, a four-sided cell disappearance leads to two different configurations and each configuration

TABLE I. Summary of all runs and initial configurations for normal foam simulations

Run	Initial network[a]	Initially assigned pressure[b] (atm)	Initial foam parameters μ_2	μ_2^A	P_0 (atm)	Note
i	Voronoi,	10^{-4}	1.891	0.606	10^{-4}	
ii	no hard-core				10^{-3}	
iii	($\mu_2=1.889$,				10^{-2}	
iv	$\mu_2^A=0.314$)	10^{-2}	1.762	0.316	10^{-2}	
v		10^{-4}	1.455	0.457	10^{-4}	
vi	Voronoi,				10^{-3}	
vii	small hard-core				10^{-2}	
viii	($\mu_2=1.469$,	10^{-2}	1.346	0.226	10^{-2}	
ix	$\mu_2^A=0.225$)				10^{-2}	large error controls[c]
x				10^{-2}	high μ_2[c]	
xi				10^{-2}	low μ_2[c]	
xii	Voronoi,	10^{-4}	0.945	0.138	10^{-4}	
xiii	large hard-core				10^{-3}	
xiv	($\mu_2=0.945$,				10^{-2}	
xv	$\mu_2^A=0.060$)	10^{-2}	0.938	0.060	10^{-2}	
xvi			0.230	0.142	10^{-2}	backward diffusion[d]
	Perfect hexagons					single defect
xvii	(one edge removed)	10^{-2}	0.006	0.005	10^{-2}	propagation

[a]The μ_2 and μ_2^A values of the initial Voronoi network are given for comparison with the values found in the foam configuration after the initializing relaxation step.

[b]The initially assigned pressure to each cell to relax a nonequilibrium (Voronoi) network to an equilibrium configuration.

[c]These runs start with the same initial configuration for run viii, but with different evolution conditions.

[d]The initial configuration of this run is prepared by applying the ''backward diffusion'' to that of run xv.

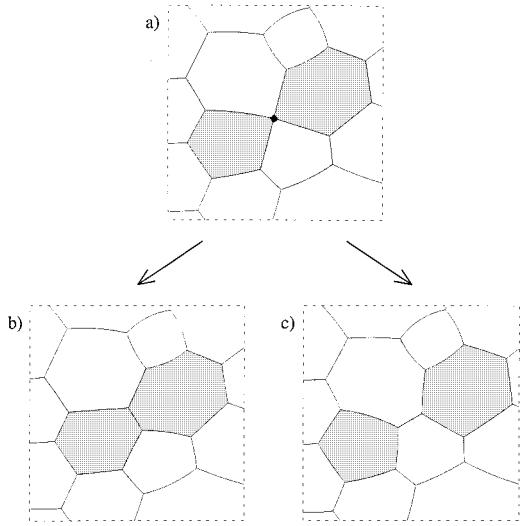

FIG. 5. Two possible configurations after four-sided cell disappearance. (a) Evolves to (b) when $\Delta\Phi_{max}=0.5°$, $\Delta\theta_{max}=0.02°$, and to (c) when $\Delta\Phi_{max}=1°$, $\Delta\theta_{max}=0.04°$. Number of bubbles of (a) is 890.

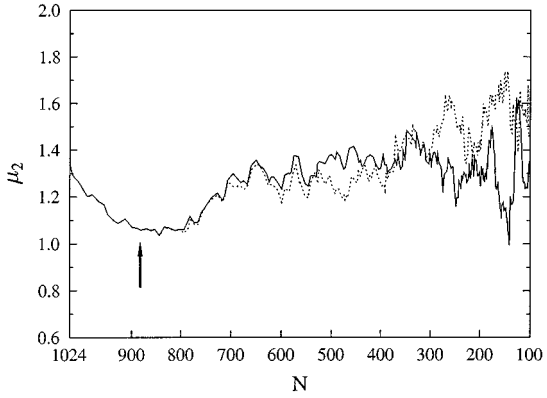

FIG. 6. μ_2 vs number of bubbles. Solid line for $\Delta\Phi_{max}=0.5°$, $\Delta\theta_{max}=0.02°$ and dotted line for $\Delta\Phi_{max}=1°$, $\Delta\theta_{max}=0.04°$. Arrow indicates the moment when the ''bifurcation'' shown in Fig. 5 occurs.

will, in turn, follow a topologically different path of evolution. In soap bubble experiments, the choice of a certain configuration after a four- or five-sided cell shrinks to zero area (leaving fourfold or fivefold vertex) depends on fast dynamical effects stemming from foam wetness, capillary instability, the appearance of conical bubbles, and possible defects on the plate surfaces [2]. By contrast, the numerical foam evolution is idealized as a two-dimensional ''dry'' froth and is effectively ''deterministic'' in that a four- or five-sided cell is reduced to a three-sided cell via (sequential) $T1$ transitions on the shortest side before disappearance. If a configuration contains a disappearing four- or five-sided cell in which more than one side has equal shortest length, the evolution is ''nondeterministic''; but this is unlikely to occur [2] and is never observed in our various runs. However, small fluctuations due, for example, to accumulated numerical errors, can cause different wall switchings in a vanishing four- or five-sided cell, which can result in completely different foam evolution paths.

In any numerical model controls on the numerical errors for the selected variables need to be introduced. For example, to find the quasiequilibrium configurations, WK iteratively solve the relevant set of equations until the root mean square of the area change, or displacement of the vertices is smaller than a given value. In the AH model, the numerical errors related to step size are an inevitable consequence of their use of a (huge) Jacobian matrix equation. In our model, during the readjustment of the curvature, the maximum deviation $\Delta\theta_{max}$ in the opening angle of an edge from the quasiequilibrium value is tested against a given error control. In addition, the vertices are allowed to move until the maximum angle deviation (from 120°) between neighboring edges $\Delta\Phi_{max}$ is smaller than another error control. Using various values of $\Delta\Phi_{max}$ and $\Delta\theta_{max}$, we can obtain topologically different foam evolutions from one initial configuration.

We performed two different runs from an identical initial configuration with $\Delta\Phi_{max}=0.5°$, $\Delta\theta_{max}=0.02°$ and with $\Delta\Phi_{max}=1°$, $\Delta\theta_{max}=0.04°$. The difference in topology (triggered by the different error controls) between two series of configurations is first observed when the number of bubbles is 889. Figure 5 shows the two different configurations after a four-sided cell vanishes. In spite of the difference in topology, μ_2 of these two configurations remains the same for a while as shown in Fig. 6, since the side distributions are still identical in this particular example. As the two foams evolve, the topological difference between the two configurations becomes more distinct. This is because the local differences in topology propagate in space and further topological changes, through other four- or five-sided cell disappearances, can occur at a later time. Thus as the foam evolves the overall behavior of μ_2 can show deviations of the order of 10%. (The further fluctuations for bubble numbers less than about 300 may also be related to the relative poorness of statistical measures for small bubble number.) Other numerical experiments (not shown) with tighter error controls suggest that the choice $\Delta\Phi_{max}=0.5°$, $\Delta\theta_{max}=0.02°$ is adequate for our purposes and these are used in all of our runs.

Our normal protocol for effecting a $T2$ transition on four- or five-sided bubbles is to first reduce the cell to a three-sided bubble via a sequence of (one or two, respectively) $T1$ transitions on the shortest sides. However, it is also possible—say as a result of numerical error—to effect these transitions on other sides of the cell and hence induce different topological configurations. Accordingly, in one run we made the choice that always gave the lowest subsequent μ_2 and in another, the highest subsequent μ_2. These runs are compared with the ''normal'' protocol in Fig. 7. The interesting feature here is that when the lowest μ_2 path is chosen, μ_2 does not continuously decrease but seems to attain a lower bound of about 0.7, which is well maintained in the scaling regime (considered to be the regime of approximately constant μ_2). Although this behavior is a consequence of an artificial construction, not realized in real experiments, it raises the interesting theoretical challenge of trying to predict the existence and value of such a lower bound. It is not clear what the maximal μ_2 path corresponds to; but it is interesting to note that mean-field theories [18] lead to even higher μ_2 values—which is a consequence of the way this theory chooses to handle $T2$ transitions (i.e., always elimi-

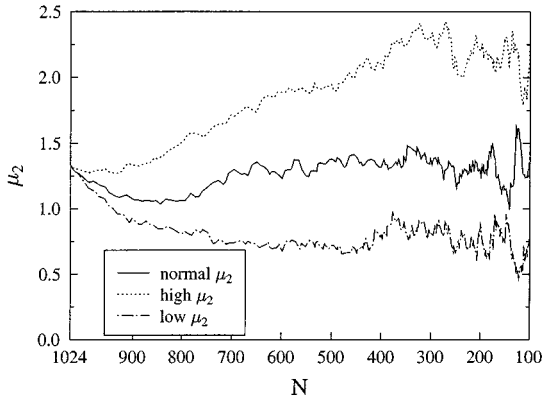

FIG. 7. The behaviors of μ_2 in ''normal,'' ''high,'' and ''low'' μ_2 models.

nating the edge from the smallest bubbles). The energetics of these different paths is also of note. Here foam ''energy'' E is defined as the total length of soap film in the entire bubble network. Thus, in the case of a perfect hexagonal foam, the energy is $E_{\rm hex}=(2\sqrt{3}NA_{\rm tot})^{1/2}$, where N is the number of bubbles and $A_{\rm tot}$ is the total area of a system [11]. As shown in Fig. 8, when we plot the ratio $E/E_{\rm hex}$, the low μ_2 path has the highest energy whereas the high μ_2 and normal μ_2 paths are much closer in energy.

C. Scaling regimes and other behaviors

The existence of a scaling regime in normal foam evolution, as well as in grain growth, has been extensively studied experimentally and by computer simulation [4,5]. One of the main ways of characterizing this regime is by following the behavior of μ_2—which should be constant during scaling behavior. In our case, extensive studies on a variety of initial conditions (runs iii, iv, vii, viii, xiv, and xv, which all have the same initial pressure $P_0=10^{-2}$ atm) show a μ_2 value in the scaling regime which fluctuates between 1.2 and 1.4 [7]. We also found that, in general, the more disordered (higher μ_2) initial foam configurations reach the scaling state faster. Our observed μ_2 is slightly higher than AH's and slightly lower than the value reported earlier in experiments [19] and simulations by Weaire and Lei [20]. This small difference is

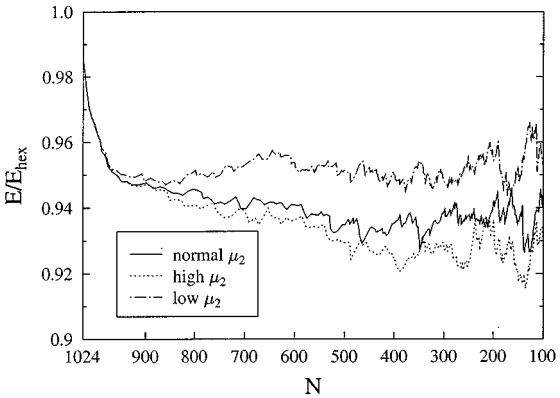

FIG. 8. The ratio of energy to $E_{\rm hex}$ vs number of bubbles in ''normal,'' ''high,'' and ''low'' μ_2 models.

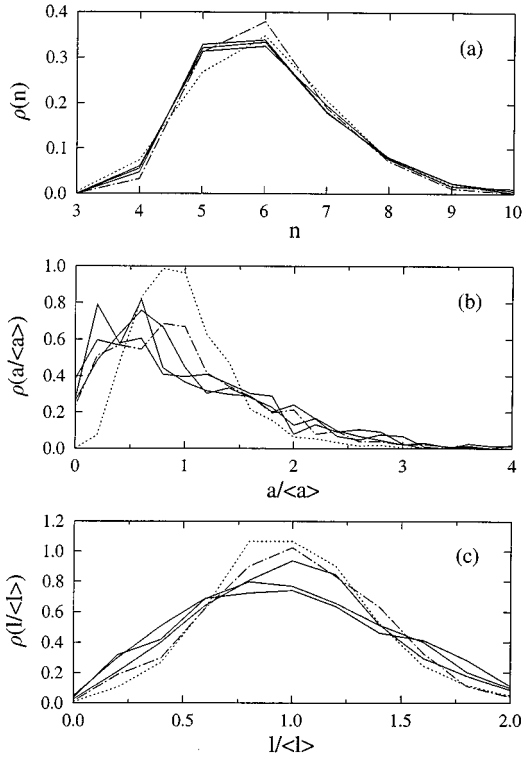

FIG. 9. (a) Side and (b) area and (c) length distributions for run viii. Dotted line is for the initial configuration, and dot-dashed line is when $N=890$ (transient state). Solid lines are for $N=660$, 520, and 380 representing the scaling state.

probably negligible considering the sensitivity of normal foam evolution to initial configuration and the numerical errors as discussed in Sec. III B.

The growth rate of the average cell area has also been a central issue in foam experiments and simulations and it is accepted that normal foams exhibit power-law growth [4,5], i.e.,

$$\langle a\rangle = A(t-t_0)^{\alpha}, \tag{13}$$

where A is a constant. In spite of the variance in measurements of α (ranging from 0.64 to 2.0) in earlier experiments [21–23,3], recent careful experimental results [24,25] indicated the growth exponent is close to one—as suggested by simple dimensional analysis. The only point we wish to make here is to emphasize the sensitivity of the exponent to fitting procedure. This is illustrated by data obtained from run viii. Fitting directly with Eq. (13) (since determining α in a log-log plot is likely to have systemetic errors [4]), we found that α is 1.02 ± 0.02 using the data between 750 and 200 bubbles and 1.26 ± 0.07 when the range is reduced to $700-300$. Clearly, reliable calculation of the growth exponent requires simulations of large systems.

The scaling regime, by definition, is characterized by the constancy of all distributions, such as the side number and normalized area distributions. As shown in Fig. 9, side distributions are clearly stationary in the scaling regime. This type of behavior is observed in most other numerical studies although we see $\rho(n=6)$ being only slightly higher than $\rho(n=5)$, whereas AH observed a more noticeable difference

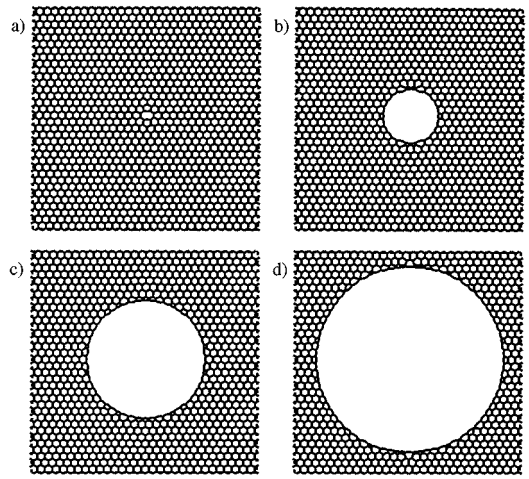

FIG. 10. Sequence of configurations for the propagation of a single defect, when (a) $t=0$, (b) $t=50$, (c) $t=100$, and (d) $t=150$. Initial number of bubbles is 1019 and the unit of time is arbitrary.

between them. Again, our results lie between AH's and experimental results [3] in which $\rho(n=6)<\rho(n=5)$. By contrast, although $\rho(a/\langle a\rangle)$ in the initial and transient states can be distinguished from that in a scaling state, it is difficult to claim that $\rho(a/\langle a\rangle)$ is stationary in the scaling regime, which might be due to the limited data. The behavior of $\rho(a/\langle a\rangle)$ is not reported in the AH and WK studies. We also show the normalized edge-length distribution $\rho(l/\langle l\rangle)$ that exhibits some degree of stationarity. Later we will see that this distribution function has special properties in the case of breaking foam evolution.

In complete contrast to the above, single defect propagation in a perfect hexagonal foam is one example in which normal foam evolution never reaches a scaling state. Although we were drawn to this problem because of its partial analogy to front propagation in solidification, it has also been considered recently in [26] where it was claimed that in a mean field model, scaling behavior could occur.

In our simulation, a single defect is generated by eliminating one edge from a perfect hexagonal lattice, and this structure is relaxed to an equilibrium initial configuration, which is shown in Fig. 10(a). Driven by von Neumann's law, the initial eight-sided bubble, surrounded by two five-sided bubbles and six hexagons, will grow continuously; conversely, the two five-sided bubbles will shrink. These dynamics generate the outward propagation of an area unpopulated by bubbles. The growth rate of the central area in Fig. 10 can be predicted by von Neumann's law. Using the radius of the central area r_c, Eq. (2) becomes $d(r_c^2)/dt \propto n_c$, where the number of sides, n_c, of this area is large. Since n_c is proportional to r_c, dr_c/dt is constant. As shown in Fig. 11, the result of our simulation shows linear growth of the radius, as expected. A very similar calculation was also reported recently by Yi, Mombach, and Glazier [27] using a Potts model code. In their simulations, the evolving front is less symmetric and shows what are probably a few spurious large bubbles in the ''melting'' domain—undoubtably an artifact of the Potts model representation. In fact the highly symmetric evolution that we observe also provides an additional test of our code and the error controls since no symmetry is incorporated in the edge and vertex movement steps.

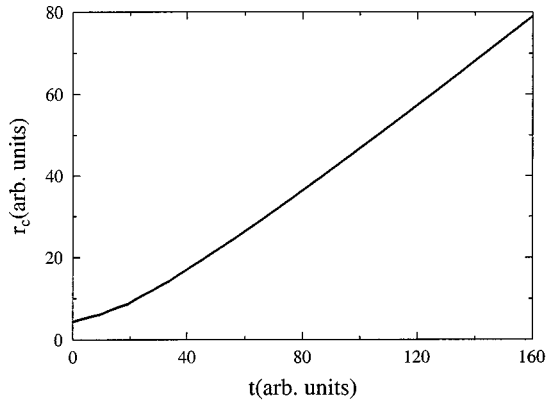

FIG. 11. The radius of the big center bubble, r_c vs time in the propagation of a single defect.

Finally, in our studies of normal foams we have carried out extensive investigations of Lewis's law [28], which claims a linear relationship between the mean area of an n-sided cell and the side number; and the Aboav-Weaire law [23,29,30] which gives a semiempirical relationship for the average number of sides of the cells that are neighbors to an n-sided cell. Our numerical results [7] all agree closely with those found in other studies (see, for example, [24,11]).

IV. NUMERICAL RESULTS FOR BREAKING FOAM EVOLUTION

The phenomenon of wall rupture, although it has been commonly observed in normal foams [24], grain growth [22,31], and magnetic garnet films [32], has not been studied in detail due to its complexity and the relatively small contribution it makes to the statistical quantities measured in those experiments. The first experiment devoted solely to this subject was recently performed by Burnett *et al.* [15] and our simulation studies were motivated by this experimental work. In this experiment, wall rupture was initiated by gentle heating from a light box underneath the experimental cell, and at a critical ''breaking time'' (which depends on the temperature ramping rate) a large-scale mechanical cascade of wall rupture was observed. In this ''cascade regime,'' it was found that the mean edge length grew linearly in time and the associated edge-length distributions were effectively stationary.

In principle, the evolution of a breaking foam can be completely determined if the exact time and location of each breakage is known. However, the modeling of a breaking foam is still at a relatively primitive stage since the dynamics of wall rupture, which involves many complex physicochemical issues, is not well understood, and the available experimental results are limited to those mentioned above. In Sec. II B, we postulated three breaking rules in which the probability to break the ith edge is given by

$$\mathrm{Prob}_i \propto (l_i)^z, \tag{14}$$

where l_i is the length of ith edge and z takes values 0, 1, and

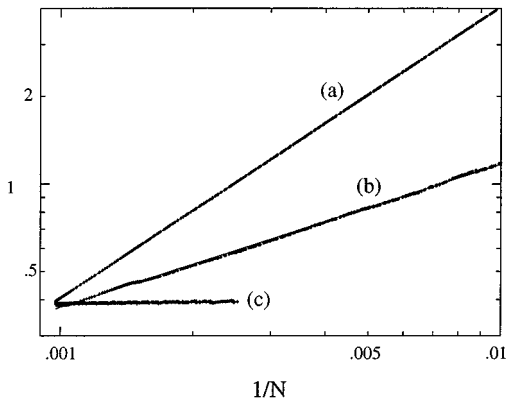

FIG. 12. (a) $\langle a \rangle$ vs $1/N$ for run xv. By definition of the mean area, the ''evolution exponent'' for mean area is always one. $\langle l \rangle$ vs $1/N$ for (b) run xv; and (c) run xvii (a single defect propagation). The dimension of the system is scaled such that initial value of $\langle l \rangle$ is the same as that of $\langle a \rangle$ for run xv.

2 for each breaking rule. Here, we will test the validity of these breaking rules by comparing the numerical results with the experimental ones.

Traditionally, the evolution of a froth is characterized by following the behavior of various quantities, such as mean area growth, μ_2, various probability distributions, etc., as a function of either time or the number of bubbles. However, since it is only the breaking rules, and not the time interval between successive wall breaks that are being tested against the experimental results, we need some notion of the topological evolution without involving the time variable explicitly. The apparent difference in topology between a normal and breaking foam can be characterized by the ''homogeneity'' of the spatial structure. Namely, a breakage tends to drive the pattern of a foam toward an inhomogeneous appearance, while the normal foam tends to retain some degree of homogeneity. (A single defect propagation in a normal foam being one exception.) The topological evolution can be characterized by the changes in homogeneity that are related to the energy or mean edge length of a system. Rather than attempt to follow these changes as a function of time, we follow them as a function of bubble number. For any coarsening system, the mean area is proportional to $1/N$ by definition, namely,

$$\langle a \rangle = A_{\mathrm{tot}} \left(\frac{1}{N} \right), \tag{15}$$

where A_{tot} is the total area of a system and N the total number of bubbles. Accordingly, we have proposed [15] a power-law evolution for the mean edge length in terms of $1/N$, i.e.,

$$\langle l \rangle \propto \left(\frac{1}{N} \right)^{\beta} \tag{16}$$

where β denotes the ''evolution exponent'' of the mean edge length.

As shown in Fig. 12, for a *normal* form with initial Voronoi configuration, $\langle l \rangle$ satisfies Eq. (16) quite well and β is found between 0.48 and 0.50. For a single defect propagation by contrast, β is 0.016, with a negligible standard deviation that corresponds to a structure evolving towards extreme inhomogeneity. If we regard these behaviors of normal foam relaxation and single defect propagation, respectively, as the two extremes of homogeneous and inhomogeneous structures, we would expect β for a breaking foam to lie between 0 and 0.5. For each breaking rule, we choose the two initial configurations that were used for runs xv and iv of a normal foam. We label the breaking foam runs with less disordered initial configuration (used in run xv) as runs I, II, and III corresponding to each breaking rule $z=0$, 1, and 2, respectively, and the runs with more disordered initial configuration (used in run iv) as runs IV, V, and VI.

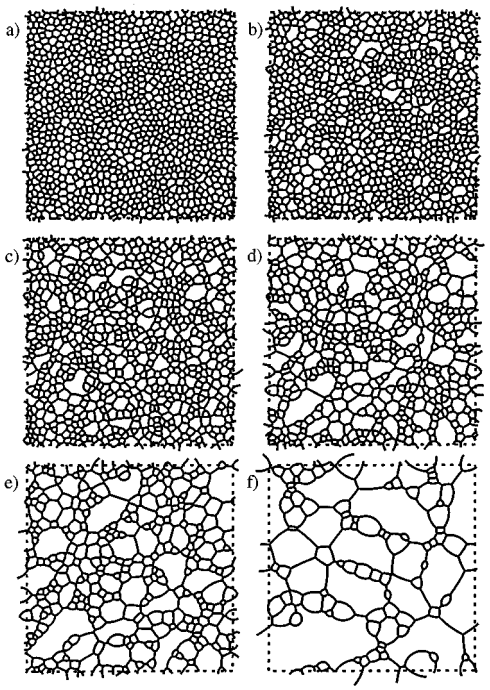

FIG. 13. Sequence of configurations for run I. Number of bubbles in (a)–(f) are 1024, 880, 710, 500, 310, and 100.

A. Evolution topology

In order to get an overall picture of the evolution of breaking foams, it is helpful to look at a sequence of ''frames'' for the different breaking rules. These are shown in Figs. 13–15 in which all foams start with the identical initial structure whose μ_2 is similar to that of the initial foam used in the experimental work [15]. In all three figures, we see the progressive enlargement, due to wall breakage, of various bubbles that eventually become surrounded by clusters of small bubbles. Tracking this process frame by frame (i.e., a movie) clearly shows long-range correlations, i.e., a wall breakage in one region triggering a movement some distance away, which are often accompanied by successive $T1$ processes. A noteworthy feature of the simulations is the frequent appearance of two-sided bubbles; just as in the experimental studies of breaking foams (and virtually never in normal foams). A two-sided bubble, generated from a three-sided bubble that loses a neighboring edge (due to breakage), appears to be stable unless a nearby bubble moves close enough to induce a wall switching.

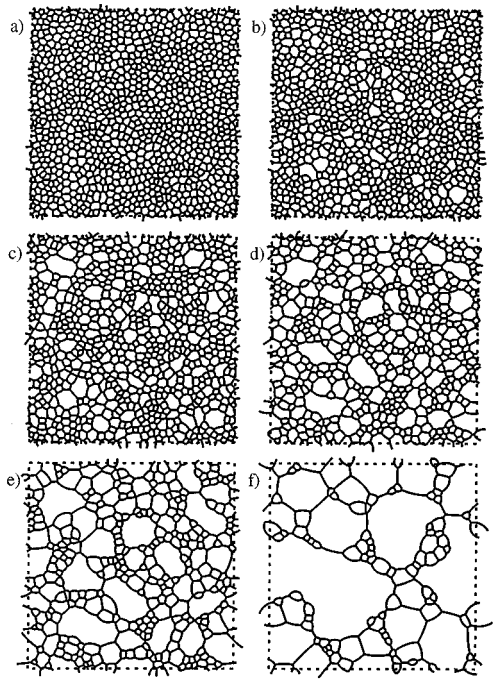

FIG. 14. Sequence of configurations for run II. Number of bubbles in (a)–(f) are 1024, 880, 710, 500, 310, and 100.

Although the phenomena described above for each breaking rule generally agree to some extent with the experimental observation, there are clear differences in evolving patterns for the different breaking rules. The evolution for the random breaking rule ($z=0$) seems to be different from the experimental pattern evolution in that more long edges and less small bubbles survive at later stages. It is, however, difficult to compare qualitatively the evolution with breaking rule $z=1$ or 2 with that of the experiment; a detailed quantitative comparison will be discussed in Sec. III B. In Fig. 16, we show an evolution sequence that starts with a more disordered initial structure with the breaking rule $z=1$ (run V). These sequential frames indicate that the evolution of a breaking foam is sensitive to the initial foam structure; at least for those breaking rules, that depends in some way on the length of the edge.

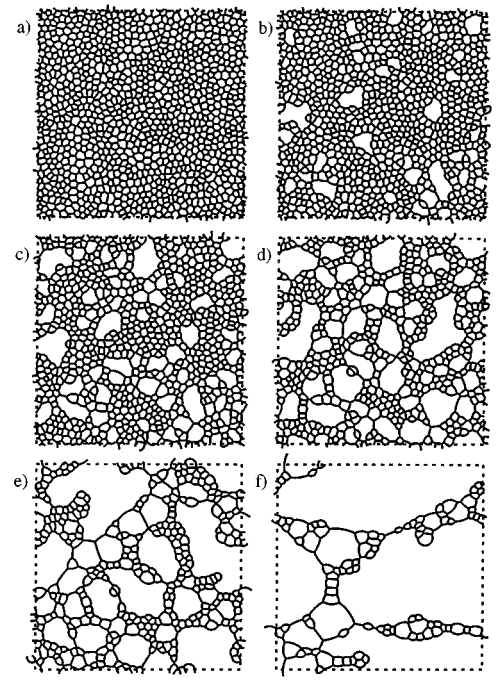

FIG. 15. Sequence of configurations for run III. Number of bubbles in (a)–(f) are 1024, 880, 710, 500, 310, and 100.

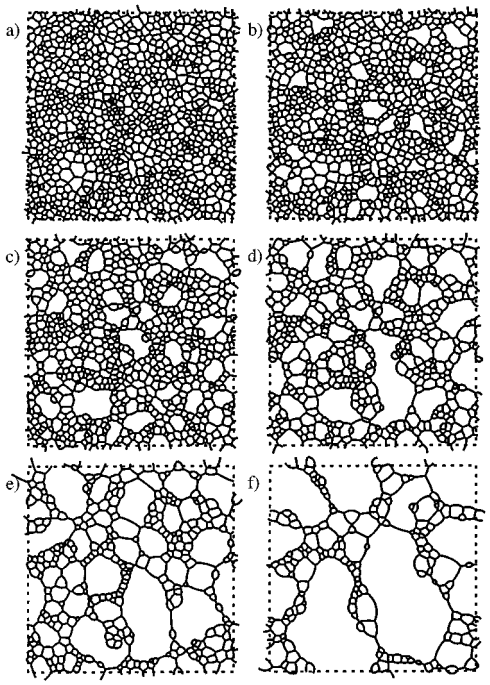

FIG. 16. Sequence of configurations for run V. Number of bubbles in (a)–(f) are 1024, 880, 710, 500, 310, and 171.

B. $\langle l \rangle$ behavior

As discussed before, one way to characterize a two-dimensional coarsening cellular system is through various evolution exponents. By using Eq. (15) in Eq. (16) we see the relationship

$$\langle l \rangle \propto \langle a \rangle^{\beta}. \tag{17}$$

In the case of normal foam evolution (excluding pathological cases such as single defect propagation shown in Sec. III C), we know that the bubble area scales like $\langle l \rangle^2$ (i.e., the bubble length scale set by $a^{1/2}$ is the same length scale as that set by the edge length) and hence $\beta=0.5$. However, in a breaking foam, the length scale set by a typical bubble edge is no longer the same as that set by the square root of the bubble area. Accordingly, we can no longer expect $\beta=0.5$ and, based on the observation that the typical structure is that of a (very) large bubble made up of many short sides, we would expect $\beta<0.5$. Experimentally, the observed values ranged from 0.25 to 0.32 [15].

We show log-log plots of $\langle l \rangle$ as a function of $1/N$ in Fig. 17, in which the power law in Eq. (16) is well satisfied for all runs except run VI, and the fitted values of β from these plots are summarized in Table II. With the random breaking rule, regardless of the initial foam structure, we obtain

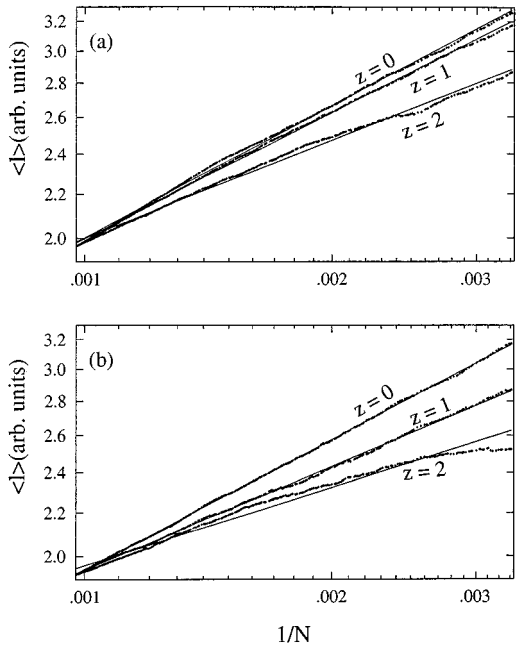

FIG. 17. Log-log plot of $\langle l \rangle$ vs $1/N$ for (a) runs I–III and (b) runs IV–VI.

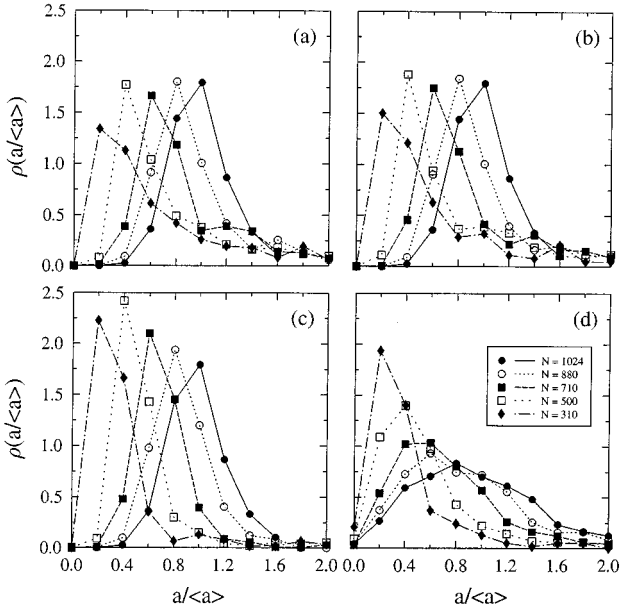

FIG. 18. Area distributions for runs (a) I, (b) II, (c) III, and (d) V.

$\beta = 0.41$, which is higher than the experimental value. These high evolution exponents, together with the differences in topology of the evolving patterns described in Sec. IV A, lead us to conclude that wall breakages do not occur at random in a breaking foam. Since β is sensitive to the initial foam structure for the breaking rules $z = 1$ and $z = 2$, the evolution exponents for runs II and III, whose initial μ_2 is similar to that of the experimental foam, are compared with the experimental results. This indicates that the breaking rule $z = 2$ represents the dynamics of a breaking foam more closely than the breaking rule $z = 1$. In Sec. II B, the breaking rule $z = 1$ was proposed based on the empirical observation that the probability to rupture a *static* single soap film, within a given time interval, is proportional to its surface area. Therefore, we suspect that the movement of a soap film, including expansion or shrinkage, also affects its probability to rupture.

C. Probability distributions

In the case of a normal foam, the probability distributions of side, area, and edge length were used in order to show the existence of the scaling regime, in which these distributions are stationary. By contrast, in a breaking foam, the peaks of the area and side distributions shift towards smaller values as shown in Figs. 18 and 19. In the side distribution, it is interesting that $\rho(n)$ always increases when $n < 5$ and decreases when $5 < n < 8$ (9 for run V) and eventually the four-sided bubbles are dominant. However, the length distributions show somewhat different behavior from the area and side distributions as shown in Fig. 20. Although the length distributions for runs I–III which start with a narrow length distribution, show a small transition, overall they seem to be stationary—which is consistent with the experimental observation [15].

TABLE II. ''Evolution exponent'' for all runs in the breaking foam simulations. These exponents are obtained with negligible standard deviations by fitting the data in the range of $N = 1024$–300.

Run	I	II	III	IV	V	VI
	0.412	0.394	0.306	0.409	0.325	0.245

V. CONCLUSIONS

We have developed a new algorithm that can deliver efficient and accurate simulations of two-dimensional dry

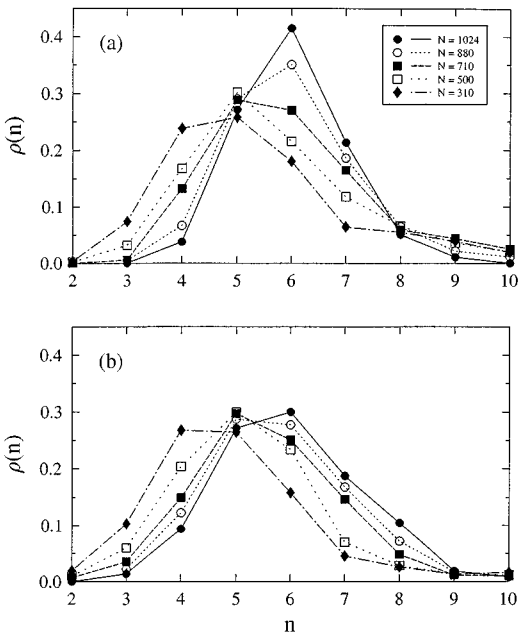

FIG. 19. Side distributions for runs (a) II and (b) V.

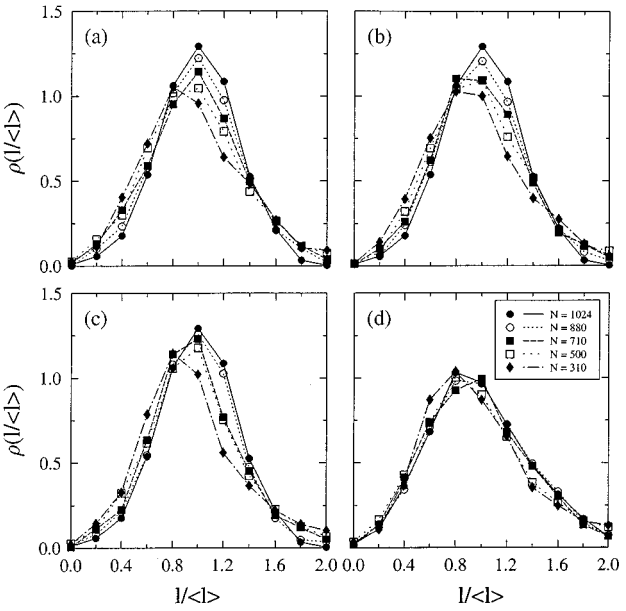

FIG. 20. Length distributions for runs (a) I, (b) II, (c) III, and (d) V.

foams. Overall, our results for a normal foam using this algorithm are in broad agreement with those by WK and AH except for a few cases in which our values of quantities such as μ_2 and various probability distributions lie between those of WK and AH. The fact that our algorithm tracks the movement of all edges and vertices at any instant enables the chaotic behavior triggered by numerical errors to be investigated. It is very likely that these ''stochastic'' effects are a source of the small discrepancies found among the physically realistic computational models, namely, WK, AH, and ours. Breaking foams have been simulated using this algorithm and compared with the recent experimental work [15]. In spite of the lack of understanding of the precise breaking mechanism, the simulation results with the breaking rule $z=2$ show similar evolution topologies and growth exponents to those seen in the experiments.

Finally, we comment that since the (individually stored) surface tension of each edge is independent of the overall simulation procedure, the code can be easily modified for systems in which the surface tension of each edge varies. This makes it fairly easy to study anisotropic grain growth in which the surface energy varies as a function of orientation between adjacent cells [7].

ACKNOWLEDGMENTS

This work was supported by U.S. Department of Energy (DOE) Grant No. DE-FG03-93ER25174. The authors thank Y. Tam for his continuous encouragement and interest in this project and G. D. Burnett for help in preparing the manuscript. The authors also thank R. M. C. de Almeida for considerable assistance in revising the text.

[1] J. von Neumann, in *Metal Interfaces*, edited by C. Herring (American Society for Metals, Cleveland, OH, 1952), p. 108.
[2] V. Fradkov, M. Magnasco, D. Udler, and D. Weaire, Philos. Mag. Lett. **67**, 203 (1993).
[3] J. Glazier, Ph.D. thesis, University of Chicago, 1989 (unpublished).
[4] J. Glazier and D. Weaire, J. Phys. Condens. Matter **4**, 1867 (1992).
[5] J. Stavans, Rep. Prog. Phys. **56**, 733 (1993).
[6] F. Bolton and D. Weaire, Philos. Mag. B **63**, 795 (1991); **65**, 473 (1992); S. Hutzler, D. Weaire, and F. Bolton, *ibid*. **71**, 277 (1995).
[7] J. J. Chae, Ph.D. thesis, University of Arizona, 1995 (unpublished).
[8] D. Weaire and J. Kermode, Philos. Mag. B **48**, 245 (1983); **47**, L29 (1983); **50**, 379 (1984).
[9] J. Kermode and D. Weaire, Comput. Phys. Commun. **60**, 75 (1990).
[10] H. Aref and T. Herdtle, in *Topological Fluid Mechanics*, edited by H. Moffatt and A. Tsinober (Cambridge University Press, Cambridge, England, 1990), pp. 745–764.
[11] T. Herdtle and H. Aref, J. Fluid Mech. **241**, 233 (1992).
[12] K. Kawasaki and Y. Enomoto, Physica A **150**, 463 (1988).
[13] K. Nakashima, T. Nagai, and K. Kawasaki, J. Stat. Phys. **57**, 759 (1989).
[14] R. Fullman, in *Metal Interfaces*, edited by C. Herring (American Society for Metals, Cleveland, OH, 1952), p. 179.
[15] G. Burnett *et al.*, Phys. Rev. E **51**, 5788 (1995).
[16] J. Bikerman, *Foams* (Springer-Verlag, New York, 1973), pp. 71 and 231.
[17] D. Weaire and N. Rivier, Contemp. Phys. **25**, 59 (1984).
[18] M. Marder, Phys. Rev. A **36**, 438 (1987).
[19] J. Stavans and J. Glazier, Phys. Rev. Lett. **62**, 1318 (1989).
[20] D. Weaire and H. Lei, Philos. Mag. Lett. **62**, 427 (1990).
[21] C. Smith, in *Metal Interfaces*, edited by C. Herring (American Society for Metals, Cleveland, OH, 1952), pp. 65–108.
[22] C. Smith, Metall. Rev. **9**, 1 (1964).
[23] D. Aboav, Metallography **3**, 383 (1970).
[24] J. Glazier, M. Anderson, and G. Grest, Philos. Mag. B **62**, 615 (1990).
[25] J. Stavans, Phys. Rev. A **42**, 5049 (1990).
[26] B. Levitan, Phys. Rev. Lett. **72**, 4057 (1994).
[27] J. Yi, J. M. C. Mombach, and J. Glazier, Phys. Rev. E **52**, 3333 (1995).
[28] F. Lewis, Anat. Rec. **38**, 341 (1928).
[29] D. Weaire, Metallography **7**, 157 (1974).
[30] D. Aboav, Metallography **13**, 43 (1980).
[31] M. Anderson, D. Srolovitz, G. Grest, and P. Sahni, Acta Metall. **32**, 783 (1984).
[32] K. Babcock and R. Westervelt, Phys. Rev. Lett. **63**, 175 (1989).